

Quasi normal modes of a Casimir-like traversable wormhole through the semi-analytical WKB approach.

R. Avalos* and E. Contreras†

*Departamento de Física, Colegio de Ciencias e Ingeniería,
Universidad San Francisco de Quito,
Quito 170901, Ecuador.*

In this work, we implement the semi-analytical WKB method to explore the behaviour of a scalar field on a traversable wormhole space-time with a Casimir-like complexity reported in Eur. Phys. J. C 82, 420 (2022). We estimate the error in the computation of the quasi-normal frequencies of the scalar field at each order in the WKB and show that the order with the best accuracy is not unique. We compute the value of the quasinormal frequencies for the smallest estimated error. As an aside, we find that the imaginary part of the quasinormal modes frequencies approach to zero for the fundamental mode mimicking the so-called quasi-resonance observed for massive scalar fields in the Reissner-Nordström background.

Keywords: QNM

I. INTRODUCTION

Undoubtedly, the study of traversable wormholes (TW's) [1–18] is an attractive research area not only for the intriguing features they encode regarding the possibility of interstellar travels but for their potential as black hole mimickers as has been established in recent years [19–21]. On the one hand, the analysis of how a TW responds to perturbations allows one to extract useful information about its similitude with the ringdown phase of a black hole through its quasinormal modes (QNM) spectrum. On the other hand, the behaviour of QNM frequencies can be related to the stability of the perturbing field itself as its imaginary part, $Im(\omega)$, is related to the damping factor associated with the loss of energy through gravitational radiation. Indeed, depending on the sign of $Im(\omega)$ (see Eq. (5)) the perturbation either grows exponentially leading to instabilities or decreases monotonously.

The study of the QNM can be carried out by different methods (for an incomplete list see [22–39] and references therein, for example). Nevertheless, in this work, we shall implement the semi-analytical WKB approximation reported in [40]. In particular, we analyse the QNM for the TW reported in [41] that fulfills all the basic requirements of a TW, namely, flaring out condition, small tidal forces, reasonable time to traverse the throat and, an arbitrarily small amount of exotic matter. It is worth mentioning that, although the solution in [41] depends on a free parameter which is bounded in accordance to the above mentioned requirements, it is our main goal here to analyse the possibility of refining such an interval by exploring the stability of the scalar perturbation. It should be emphasized that this is the first study on QNM for this solution in the literature.

This work is organized as follows. In the next section we introduce the computation of the QNM frequencies by the WKB approximation. Next, in section III, we review the main aspects of the TW with Casimir-like complexity reported in [41]. The results obtained in this work are entirely contained in section IV where we discuss their impact and scope. It is worth mentioning that all of our computations were performed with the Mathematica notebook publicly available in <https://goo.gl/nykYGL>. In the last section we conclude the work.

II. QNM BY THE WKB APPROXIMATION

Let us start by considering the standard line element of a TW in spherical coordinates given by [1]

$$ds^2 = -e^{2\phi} dt^2 + dr^2/(1-b/r) + r^2(d\theta^2 + \sin^2\theta d\phi^2), \quad (1)$$

where $\phi = \phi(r)$ is the redshift function which encodes information on the radial tidal force and $b = b(r)$ is the shape function which enciphers the main features of the throat of the TW.

It is well known that we can perturb a TW by considering small deviations in the space-time background or by studying the evolution of test fields in the underlying geometry. Remarkably, whatever the path we follow, the behaviour of the perturbation field is governed by a Schrödinger-like equation, namely

$$\left(\frac{d^2}{dr_*^2} + \omega^2 - V(r_*) \right) \chi(r_*) = 0, \quad (2)$$

where

$$r_*(r) = \int_{r_0}^r \frac{1}{\sqrt{1-b(r')/r'}} dr', \quad (3)$$

is the tortoise coordinate and $V(r)$ is the effective potential whose functional profile depends on the particular metric given by Eq. (1). It is worth noticing that, as

* ravalos@usfq.edu.ec

† econtreras@usfq.edu.ec

$r_* \in (-\infty, \infty)$, the throat of the wormhole is at $r_* = 0$ and the asymptotically flat region far from the throat corresponds to $r_* = \pm\infty$. In this manuscript, we shall perturb the TW geometry with a massless scalar field, so the potential corresponds to

$$V_L(r) = e^{2\phi} \left(\frac{L(L+1)}{r^2} - \frac{r b' - b}{2r^3} + \frac{\phi'}{r} \left(1 - \frac{b}{r} \right) \right), \quad (4)$$

where L represents the multipole number.

We are looking for solutions of (2) such that the wave is purely out-going when we approach to infinity, namely

$$\chi(r_*) \sim C_{\pm} \exp(\pm i\omega r_*), \quad r_* \rightarrow \pm\infty. \quad (5)$$

In this case, the solution is called a QNM with $\omega = \text{Re}(\omega) + i\text{Im}(\omega)$. It is clear that the QNM frequencies encode valuable information about the evolution of the perturbation field. Indeed, it is well-known that, on the one hand, the real part of ω gives information about the oscillation of the signal and, on the other hand, the imaginary part $\text{Im}(\omega)$ accounts for the damping factor associated to the energy loss by gravitational radiation. Even more, when $\text{Im}(\omega) > 0$, the perturbation is unstable given that the growth of the perturbation field is exponential so to ensure the stability we demand that $\text{Im}(\omega) < 0$.

Although the QNM frequencies can be computed by numerical methods, in this work, we shall take advantage of the fact that Eq. (2) coincides formally with the one-dimensional Schrödinger equation which is the preferred arena to implement the well-known WKB approximation. It is worth mentioning that this strategy was introduced in Ref. [42] and has been refined to higher orders in [40] to deal with perturbations of black hole geometries. As such, the same strategy has been adopted to work the problem of TW with bell-shaped potentials in [36]. In any case, the formula for the computation of the QNM frequencies to the k^{th} order in perturbation reads

$$i \frac{\omega^2 - V_0}{\sqrt{-2V_0''}} - \sum_{j=2}^k \Lambda_j = k + \frac{1}{2}, \quad (6)$$

where V_0 and V_0'' stand for the maximum of the potential and its second derivative respect to the tortoise coordinate, respectively. In the case of TW with bell-shaped potentials (see Fig. 1), the maximum is located at the throat ($r = r_0$, $r_* = 0$). Finally, Λ_j contains all the higher order corrections and can be found in [40]. In Eq. (6), k is the order of the WKB. It should be emphasized that, an increasing in k does not necessarily lead to a better approximation of the quasinormal frequencies. To be more precise, the order k leading to the best value of ω is not unique but could depend on the pair (n, L) chosen. For that reason, in this work we shall implement the following strategy for the computation of the best ω for each order:

1. We estimate the accuracy by using [40]

$$\Delta_k = \frac{|\omega_{k+1} - \omega_{k-1}|}{2}, \quad (7)$$

which, as discussed in [40], is usually greater than the error, namely

$$\Delta_k \geq |\omega - \omega_k|. \quad (8)$$

with ω the accurate value of the quasinormal frequency. From (8) we see that as $\Delta_k \rightarrow 0$ for some k , the accuracy of the WKB increases.

2. We compute $\text{Im}(\omega)$ and $\text{Re}(\omega)$ with the smallest Δ_k associated to a given pair (n, L) .

In the next section we briefly introduce the TW solution in which we will focus our analysis

III. THE MODEL

The model we are interesting in here corresponds to the TW with Casimir-like complexity supported by a arbitrarily small amount of exotic matter which metric is given by [41]

$$\begin{aligned} \phi(r) &= \ln \left(\frac{c_0 r}{c_0 r + r_0} \right) \\ b(r) &= \frac{2r_0}{c_0} + \left(1 - \frac{2}{c_0} \right. \\ &\quad \left. - \frac{4[4 - 2c_0 + \ln(1 + \frac{1}{c_0})](c_0^2 - 2c_0 - 3)]}{c_0[-3 - 4c_0 + 4c_0(c_0 + 1)\ln(1 + \frac{1}{c_0})]} \right) \frac{r_0^2}{r} \\ &\quad + \frac{4[4 - 2c_0 + \ln(1 + \frac{1}{c_0})](c_0^2 - 2c_0 - 3)]}{c_0[-3 - 4c_0 + 4c_0(c_0 + 1)\ln(1 + \frac{1}{c_0})]} \frac{r_0^3}{r^2} \end{aligned} \quad (9)$$

where c_0 is the only free parameter which is restricted to the values

$$0.950679 < c_0 < 4.86215. \quad (11)$$

It is worth mentioning that, the interval above ensures (see [41] for details): i) a finite time of travel while traversing the wormhole, ii) a reasonable values for the radial tidal force and iii) an arbitrarily small amount of exotic matter. Although the solution has been analysed in some detail in [41], in the next section we complement it by exploring its response to scalar perturbations.

IV. RESULTS AND DISCUSSION

In this section, we show and discuss the response of the Casimir-like TW in [41] to scalar perturbations.

In Fig. (1) it is shown the effective potential given by Eq. (4) parameterized by c_0 as a function of the tortoise coordinate r_* for different values of L . Note that the potential reaches a maximum at the throat ($r_* = 0$) as required for the implementation the WKB method¹. The

¹ In the case that there were other local maximum points this numerical method will not work.

behaviour of the potential with respect to L is clear: as L increases the height of the potential also increases. Notice that the maximum values of the potential for $L = 10$ are around one order of magnitude larger than the values for $L = 2$. Similarly, the barrier also increases as the free parameter c_0 grows.

In Tables I and II we show the values of Δ_k and $Im(\omega_k)$ for $k \in [2, 7]$, $n = 0, 1, 2$ and $L = 0, 1, 2, \dots, 10$ for different values of the free parameter c_0 . Note that, the smallest Δ_k for each pair (n, L) has been highlighted in red color. Note that as c_0 grows, the smallest Δ_k appears when k increases. Similarly, for a fixed c_0 , Δ_k reach its minimum value for bigger k as L increases. However, it should be emphasized that for small L the minimum value reached by Δ_k is considerably greater than its value for high L . For example, for $c_0 = 0.96$ and $n = 0$, the smallest error is obtained for $k = 4$ but $\Delta_4 = 0.6518$ for $L = 0$ and $\Delta_4 = 0.0068$ for $L = 10$, which corresponds to a ratio of two orders of magnitude. In this regard, we should consider the quasinormal frequency obtained for $L = 0$ as not accurate. A possible consequence of such a lack of accuracy, its that the computation of $Im(\omega)$ could lead to a positive number (indicated with a dash in Table II) which does not necessarily indicate an instability of the scalar field. What is more, the WKB cannot be used for unstable modes in principle so that positive values are meaningless. Indeed, given that the potential is positive everywhere (as shown in Fig. (1)) the stability of the scalar field is ensured. It worth mentioned that we have computed Δ_k for $k = 8, 9, 10, 11, 12$ but the error increases considerably. For this reason we have not shown this data here.

To complement the analysis, we plot both the real and the imaginary part of the QNM frequencies as a function of c_0 by setting different values of L and varying the overtone n . Furthermore, based on the above results we will perform the analysis for values of L we are confident of with our approach, namely, $L = 5, 6, \dots, 10$.

In Fig. 2 we show the $Im(\omega)$ as a function of c_0 for different values of L and n . It is worth emphasizing that, the plots are not parameterized with the same k but each point corresponds to the best WKB order. To be more precise, in order to obtain Fig. 2 we have identified the best order k from the minimum value of Δ_k from a table (not shown here) generated by setting c_0 in a step of 0.01. Higher precision is possible but the computational time increases considerably. Finally, we have computed $Im(\omega)$ for each k (associated to the minimum Δ_k) so,

as said before, not all the points in Fig. 2 corresponds to the same order. It is worth noticing that $|Im(\omega)|$ increases as c_0 increases and as a consequence, the damping factor grows with the free parameter c_0 . Even more, for $n = 0$ we observe that the damping factor is around zero for some values of c_0 mimicking a well-known effect observed for massive scalar fields in the Reissner-Nordström background, namely, the so-called quasi-resonance for the fundamental mode (see [36], for example).

In Fig. 3 we show the $Re(\omega)$ as a function of c_0 for different values of L and n following the same procedure described previously for the computation of $Im(\omega)$. In this case, we observe that the frequency of the signal increases with c_0 .

V. CONCLUSION

In this work, we obtained the frequencies of the QNM at different WKB-orders for a model of a traversable wormhole with Casimir-like complexity. All the results are shown as a function of the free parameter c_0 of this wormhole which is restricted to the values $0.950679 < c_0 < 4.86215$. It was shown that the effective potential is bell-shaped as a function of the tortoise coordinate. We estimated the error at each order and use this information to plot both the imaginary and the real part of the quasinormal frequencies at the best WKB order. We found that $|Im(\omega)|$ increases with the free parameter c_0 meaning a growing of the damping factor. In contrast, the real part of the quasinormal frequencies increases with c_0 implying an increasing in the oscillation of the signal. An interesting point that should be addressed before concluding this work is that for the fundamental mode, the $Im(\omega)$ approach to zero resembles what happened for the quasinormal modes of a massive scalar field on a Reissner-Nordström background. It would be interesting to perform a study of the QNM thorough the WKB with Padé aproximants. However, this analysis is out of the scope of this work and we leave this and other aspects to future developments.

Acknowledgments

The authors would like to acknowledge R. Konoplya for sharing his Mathematica notebook with higher order WKB corrections.

-
- [1] M. S. Morris and K. S. Thorne. Wormholes in space-time and their use for interstellar travel: A tool for teaching general relativity. *Am. J. Phys.*, 56:395–412, 1988.
 - [2] M. S. Morris, K. S. Thorne, and U. Yurtsever. Wormholes, Time Machines, and the Weak Energy Condition. *Phys. Rev. Lett.*, 61:1446–1449, 1988.

- [3] Miguel Alcubierre. *Wormholes, Warp Drives and Energy Conditions*, volume 189. Springer, 2017.
- [4] Matt Visser. *Lorentzian wormholes: From Einstein to Hawking*. 1995.
- [5] Francisco S. N. Lobo. Phantom energy traversable wormholes. *Phys. Rev. D*, 71:084011, 2005.

- [6] Remo Garattini. Casimir Wormholes. *Eur. Phys. J. C*, 79(11):951, 2019.
- [7] Zdeněk Stuchlík and Jaroslav Vrba. Epicyclic orbits in the field of Einstein–Dirac–Maxwell traversable wormholes applied to the quasiperiodic oscillations observed in microquasars and active galactic nuclei. *Eur. Phys. J. Plus*, 136(11):1127, 2021.
- [8] Kirill A. Bronnikov, Pavel E. Kashargin, and Sergey V. Sushkov. Magnetized Dusty Black Holes and Wormholes. *Universe*, 7(11):419, 2021.
- [9] Jose Luis Blázquez-Salcedo, Christian Knoll, and E. Radu. Einstein-Dirac-Maxwell wormholes: ansatz, construction and properties of symmetric solutions. 8 2021.
- [10] M. S. Churilova, R. A. Konoplya, Z. Stuchlik, and A. Zhidenko. Wormholes without exotic matter: quasinormal modes, echoes and shadows. *JCAP*, 10:010, 2021.
- [11] R. A. Konoplya and A. Zhidenko. Traversable Wormholes in General Relativity. *Phys. Rev. Lett.*, 128(9):091104, 2022.
- [12] Francisco Tello-Ortiz, S. K. Maurya, and Pedro Barguño. Minimally deformed wormholes. *Eur. Phys. J. C*, 81(5):426, 2021.
- [13] Cosimo Bambi and Dejan Stojkovic. Astrophysical Wormholes. *Universe*, 7(5):136, 2021.
- [14] Salvatore Capozziello, Orlando Luongo, and Lorenza Mauro. Traversable wormholes with vanishing sound speed in $f(R)$ gravity. *Eur. Phys. J. Plus*, 136(2):167, 2021.
- [15] Jose Luis Blázquez-Salcedo, Christian Knoll, and Eugen Radu. Traversable wormholes in Einstein-Dirac-Maxwell theory. *Phys. Rev. Lett.*, 126(10):101102, 2021.
- [16] Thomas Berry, Francisco S. N. Lobo, Alex Simpson, and Matt Visser. Thin-shell traversable wormhole crafted from a regular black hole with asymptotically Minkowski core. *Phys. Rev. D*, 102(6):064054, 2020.
- [17] Juan Maldacena and Alexey Milekhin. Humanly traversable wormholes. *Phys. Rev. D*, 103(6):066007, 2021.
- [18] Remo Garattini. Generalized Absurdly Benign Traversable Wormholes powered by Casimir Energy. *Eur. Phys. J. C*, 80(12):1172, 2020.
- [19] Pablo Bueno, Pablo A. Cano, Frederik Goelen, Thomas Hertog, and Bert Vercknocke. Echoes of Kerr-like wormholes. *Phys. Rev. D*, 97(2):024040, 2018.
- [20] Vitor Cardoso, Seth Hopper, Caio F. B. Macedo, Carlos Palenzuela, and Paolo Pani. Gravitational-wave signatures of exotic compact objects and of quantum corrections at the horizon scale. *Phys. Rev. D*, 94(8):084031, 2016.
- [21] R. A. Konoplya and A. Zhidenko. Wormholes versus black holes: quasinormal ringing at early and late times. *JCAP*, 12:043, 2016.
- [22] R. A. Konoplya and A. Zhidenko. Quasinormal ringing of general spherically symmetric parametrized black holes. 1 2022.
- [23] M. S. Churilova, R. A. Konoplya, and A. Zhidenko. Analytic formula for quasinormal modes in the near-extreme Kerr-Newman–de Sitter spacetime governed by a non-Pöschl-Teller potential. *Phys. Rev. D*, 105(8):084003, 2022.
- [24] R. A. Konoplya, A. F. Zinhailo, and Z. Stuchlik. Quasinormal modes and Hawking radiation of black holes in cubic gravity. *Phys. Rev. D*, 102(4):044023, 2020.
- [25] R. A. Konoplya and A. F. Zinhailo. Quasinormal modes, stability and shadows of a black hole in the 4D Einstein–Gauss–Bonnet gravity. *Eur. Phys. J. C*, 80(11):1049, 2020.
- [26] Roman A. Konoplya, C. Posada, Z. Stuchlík, and A. Zhidenko. Stable Schwarzschild stars as black-hole mimickers. *Phys. Rev. D*, 100(4):044027, 2019.
- [27] Angel Rincon, P. A. Gonzalez, Grigoris Panotopoulos, Joel Saavedra, and Yerko Vasquez. Quasinormal modes for a non-minimally coupled scalar field in a five-dimensional Einstein-power-Maxwell background. 12 2021.
- [28] Grigoris Panotopoulos and Ángel Rincón. Quasinormal spectra of scale-dependent Schwarzschild–de Sitter black holes. *Phys. Dark Univ.*, 31:100743, 2021.
- [29] Ángel Rincón and Victor Santos. Greybody factor and quasinormal modes of Regular Black Holes. *Eur. Phys. J. C*, 80(10):910, 2020.
- [30] Ángel Rincón and Grigoris Panotopoulos. Quasinormal modes of an improved Schwarzschild black hole. *Phys. Dark Univ.*, 30:100639, 2020.
- [31] Angel Rincon and Grigoris Panotopoulos. Quasinormal modes of black holes with a scalar hair in Einstein-Maxwell-dilaton theory. *Phys. Scripta*, 95(8):085303, 2020.
- [32] Wei Xiong, Peng Liu, Cheng-Yong Zhang, and Chao Niu. Quasi-normal modes of the Einstein-Maxwell-aether Black Hole. 12 2021.
- [33] Chao Zhang, Tao Zhu, and Anzhong Wang. Gravitational axial perturbations of Schwarzschild-like black holes in dark matter halos. *Phys. Rev. D*, 104(12):124082, 2021.
- [34] Grigoris Panotopoulos and Ángel Rincón. Quasinormal modes of five-dimensional black holes in non-commutative geometry. *Eur. Phys. J. Plus*, 135(1):33, 2020.
- [35] Chong Oh Lee, Jin Young Kim, and Mu-In Park. Quasinormal modes and stability of Einstein–Born–Infeld black holes in de Sitter space. *Eur. Phys. J. C*, 80(8):763, 2020.
- [36] M. S. Churilova, R. A. Konoplya, and A. Zhidenko. Arbitrarily long-lived quasinormal modes in a wormhole background. *Phys. Lett. B*, 802:135207, 2020.
- [37] R. Oliveira, D. M. Dantas, Victor Santos, and C. A. S. Almeida. Quasinormal modes of bumblebee wormhole. *Class. Quant. Grav.*, 36(10):105013, 2019.
- [38] Jose Luis Blázquez-Salcedo, Xiao Yan Chew, and Jutta Kunz. Scalar and axial quasinormal modes of massive static phantom wormholes. *Phys. Rev. D*, 98(4):044035, 2018.
- [39] Grigoris Panotopoulos and Ángel Rincón. Quasinormal modes of black holes in Einstein-power-Maxwell theory. *Int. J. Mod. Phys. D*, 27(03):1850034, 2017.
- [40] R. A. Konoplya, A. Zhidenko, and A. F. Zinhailo. Higher order WKB formula for quasinormal modes and greybody factors: recipes for quick and accurate calculations. *Class. Quant. Grav.*, 36:155002, 2019.
- [41] R. Avalos, E. Fuenmayor, and E. Contreras. Traversable wormholes with like-Casimir complexity supported with arbitrarily small amount of exotic matter. *Eur. Phys. J. C*, 82(5):420, 2022.
- [42] Bernard F. Schutz and Clifford M. Will. BLACK HOLE NORMAL MODES: A SEMIANALYTIC APPROACH.

Astrophys. J. Lett., 291:L33–L36, 1985.

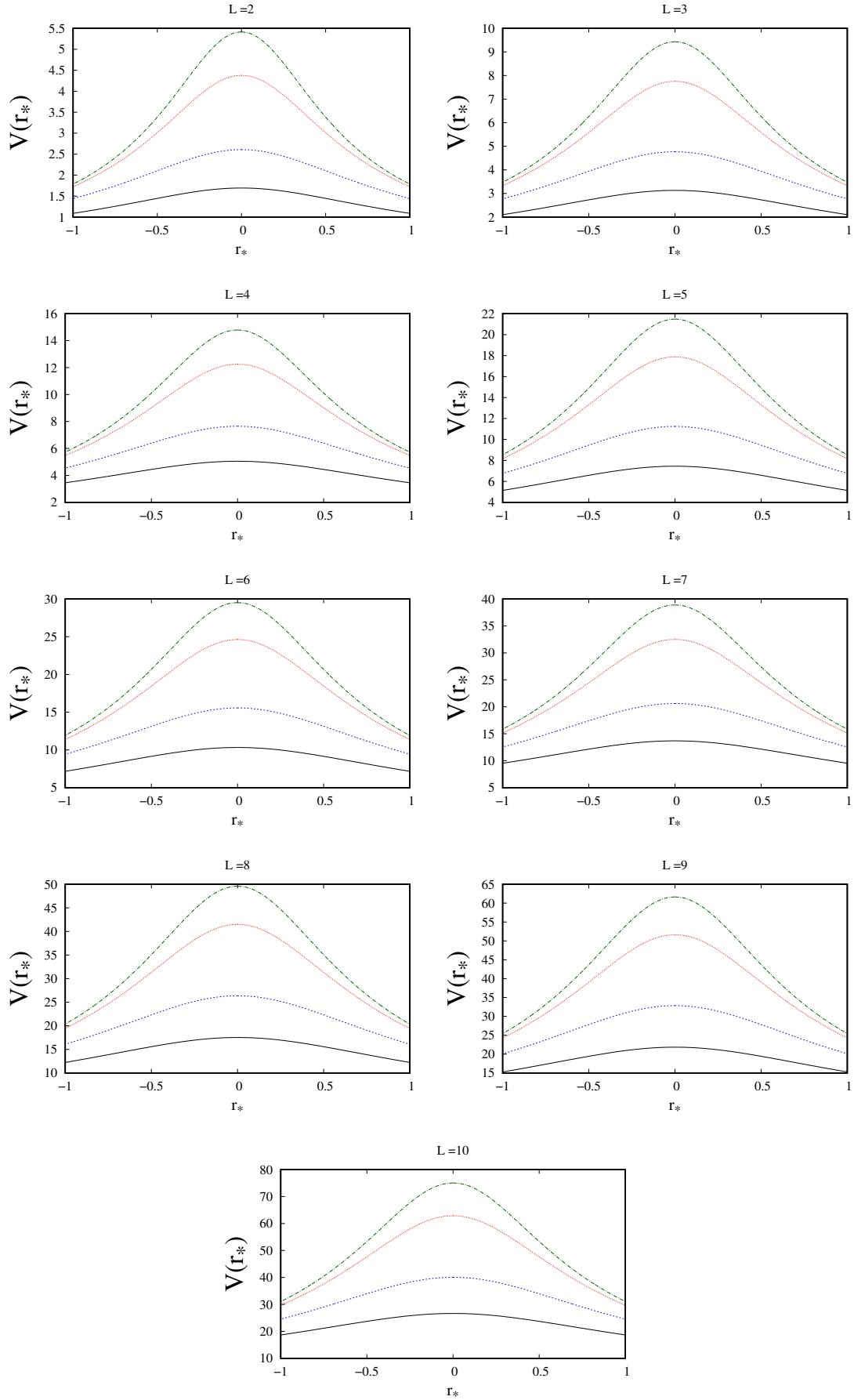


FIG. 1. Effective potential of the QNM for the wormhole as a function of the tortoise coordinate r_* for different values of L and $c_0 = 0.96$ (black line), $c_0 = 1.5$ (blue line), $c_0 = 3$ (red line), $c_0 = 4.5$ (green line).

c_0	L	n	Δ_2	Δ_3	Δ_4	Δ_5	Δ_6	Δ_7
0.96	0	0	0.8550	0.9151	0.6518	0.9289	1.0371	2.7327
		1	1.8959	2.4788	2.5087	1.9295	4.5556	4.9325
		2	2.9752	5.1475	6.9424	10.5522	23.9017	43.2611
	1	0	0.06815	0.7068	0.9036	0.6302	0.7020	2.0710
		1	1.7753	2.0336	0.7251	0.8488	2.0417	3.9368
		2	2.9641	4.4068	1.2328	6.1848	5.7790	19.4865
	2	0	0.3347	0.4074	0.6926	1.2441	1.9601	2.5636
		1	1.5434	1.5309	2.0627	2.3138	2.8719	5.8893
		2	2.6514	3.0877	1.3139	0.9384	2.7061	4.9520
	3	0	0.1713	0.2018	0.3511	0.9177	1.7722	3.4042
		1	1.4050	1.0113	2.0561	2.5588	4.4838	7.7817
		2	2.3602	2.4098	3.0993	4.0485	6.1083	10.7085
	4	0	0.1094	0.1048	0.1642	0.4061	1.0116	2.0633
		1	0.6171	0.5983	0.9170	1.8061	3.6314	6.6879
		2	2.2306	1.7326	3.0042	3.7870	6.6206	12.4492
	5	0	0.0791	0.0602	0.0799	0.1618	0.4127	0.9598
		1	0.4165	0.3579	0.4890	1.0558	2.4535	4.3869
		2	1.3130	1.1551	1.5898	2.6949	5.2246	9.5597
	6	0	0.0610	0.0380	0.0423	0.0725	0.1629	0.4025
		1	0.3177	0.2284	0.2707	0.5284	1.4187	2.4720
		2	0.9260	0.7599	0.9358	1.7079	3.7901	6.4966
	7	0	0.0508	0.0259	0.0243	0.0358	0.0708	0.1667
		1	0.0508	0.0259	0.0243	0.0358	0.0708	0.1667
		2	0.7178	0.5222	0.5612	0.9985	2.6247	4.0931
	8	0	0.0432	0.0187	0.0150	0.0192	0.0337	0.0724
		1	0.2184	0.1123	0.0981	0.1411	0.2818	0.6115
		2	0.5925	0.3773	0.3518	0.5598	1.5068	2.3926
	9	0	0.0377	0.0141	0.0098	0.0111	0.0173	0.0336
		1	0.1897	0.0847	0.0642	0.0810	0.1429	0.2982
		2	0.2184	0.1123	0.0981	0.1411	0.2818	0.6115
	10	0	0.0334	0.0111	0.0068	0.0068	0.0094	0.0167
		1	0.1680	0.0661	0.0441	0.0493	0.0779	0.1510
		2	0.4459	0.2217	0.1580	0.1951	0.3551	0.7113
1.5	0	0	0.9038	0.8509	0.3751	0.2060	0.2134	0.9103
		1	2.0309	2.6646	0.3675	0.3690	0.3926	2.1817
		2	3.1466	5.2795	5.9158	6.3915	9.3943	5.84636
	1	0	0.7121	0.5060	0.7230	0.2875	0.6123	1.7541
		1	1.8803	1.9898	0.5469	0.2441	1.0674	1.8833
		2	3.0244	4.3589	0.7898	2.6737	2.4258	7.3114
	2	0	0.2476	0.2485	0.3273	0.5260	0.8961	0.8372
		1	1.7510	1.1513	1.810	1.2946	0.9145	1.7996
		2	2.7666	2.8912	1.0133	0.3890	0.4280	3.5673
	3	0	0.1414	0.1185	0.1501	0.2727	0.5895	1.0067
		1	0.7398	0.6236	0.7528	1.1439	2.3482	3.0921
		2	2.6608	1.9264	2.6575	2.4168	3.4766	4.6030
	4	0	0.0961	0.0627	0.0678	0.1085	0.2218	0.4689
		1	0.4820	0.3486	0.3824	0.6340	1.6815	2.2922
		2	1.3078	1.0869	1.0912	1.6585	3.5125	4.9771
	5	0	0.0723	0.0372	0.0333	0.0456	0.0827	0.1754
		1	0.3586	0.2115	0.1981	0.2956	0.6412	1.1594
		2	0.9647	0.6623	0.6284	0.9416	2.7046	3.3749
	6	0	0.0581	0.0243	0.0180	0.0211	0.0335	0.0652
		1	0.2872	0.1392	0.1095	0.1408	0.2523	0.4998
		2	0.7563	0.4416	0.3599	0.4944	1.2229	1.8582
	7	0	0.0486	0.0170	0.0106	0.0107	0.0149	0.0259
		1	0.2404	0.0978	0.0650	0.0723	0.1127	0.2115
		2	0.6261	0.3134	0.2165	0.2612	0.4765	0.8950
	8	0	0.0419	0.0126	0.0067	0.0059	0.0072	0.0112
		1	0.2074	0.0724	0.0412	0.0399	0.0549	0.0940
		2	0.5371	0.2333	0.1377	0.1453	0.2279	0.4177
	9	0	0.0368	0.0097	0.0045	0.0035	0.0038	0.0052
		1	0.1826	0.0557	0.0276	0.0235	0.0288	0.0445
		2	0.4719	0.1802	0.0922	0.0856	0.1190	0.2020
	10	0	0.0329	0.0077	0.0032	0.0021	0.0021	0.0026
		1	0.1633	0.0443	0.0194	0.0146	0.0161	0.0225
		2	0.4217	0.1434	0.0645	0.0531	0.0663	0.1030

TABLE I. Numerical values of Δ_k for $c_0 = 0.96$ and $c_0 = 1.5$, multipole number L and overtone n . The values highlighted in red color correspond to the minimum value of Δ_k

c_0	L	n	Δ_2	Δ_3	Δ_4	Δ_5	Δ_6	Δ_7
3	0	0	0.6308	0.4292	0.9865	0.4743	0.6121	0.5187
		1	2.6174	3.3405	0.0647	0.1875	0.1864	0.0258
		2	3.9411	6.0466	6.1787	5.1435	7.8531	9.1116
	1	0	0.5130	0.3770	0.2731	0.1796	0.4129	0.579402
		1	2.4954	2.8692	0.2091	0.2345	2.3591	2.1394
		2	3.7755	5.5622	0.4306	1.0394	7.6925	7.7568
	2	0	0.2729	0.2018	0.1641	0.1140	0.0935	0.5407
		1	1.1120	0.7857	0.4747	0.2468	0.5982	1.5273
		2	3.6226	4.3248	0.4199	0.3637	0.2410	1.7021
	3	0	0.1700	0.1063	0.0881	0.0906	0.0998	0.0878
		1	0.7934	0.5037	0.3765	0.3157	0.2427	0.3020
		2	1.7864	1.1743	0.5936	0.2717	0.2088	1.2372
	4	0	0.1199	0.0603	0.0448	0.0466	0.0604	0.0872
		1	0.5700	0.3095	0.2205	0.2208	0.2869	0.3786
		2	1.4103	0.8412	0.5129	0.4627	0.5940	0.6875
	5	0	0.0919	0.0375	0.0238	0.0225	0.0281	0.0419
		1	0.4411	0.1994	0.1250	0.1213	0.16047	0.2442
		2	1.1107	0.5749	0.3339	0.3213	0.4680	0.7215
	6	0	0.0745	0.0252	0.0136	0.0113	0.0129	0.0181
		1	0.3602	0.1363	0.0735	0.0648	0.0798	0.1192
		2	0.9085	0.4071	0.2080	0.1898	0.2606	0.4097
	7	0	0.0627	0.018	0.0083	0.0061	0.0062	0.0079
		1	0.3050	0.0983	0.0457	0.0358	0.0401	0.0557
		2	0.7701	0.2998	0.1325	0.1099	0.1380	0.2071
	8	0	0.0542	0.0135	0.0054	0.0035	0.0031	0.0036
		1	0.2648	0.0740	0.0299	0.0208	0.0210	0.0267
		2	0.6702	0.2287	0.0878	0.0653	0.0745	0.1037
	9	0	0.0477	0.0105	0.00375	0.0021	0.0017	0.0018
		1	0.2343	0.0577	0.0205	0.0127	0.0115	0.0134
		2	0.5944	0.1798	0.0605	0.0402	0.0417	0.0534
	10	0	0.0427	0.0084	0.0026	0.0013	0.0009	0.0009
		1	0.2103	0.0462	0.0146	0.0081	0.0066	0.0070
		2	0.5347	0.1449	0.0433	0.0258	0.0243	0.0286
4.86	0	0	0.6291	0.3608	0.1609	0.2547	0.2342	0.5114
		1	1.3950	0.5022	0.0403	0.1346	0.1298	0.1342
		2	4.5186	6.6421	6.6954	5.2056	7.5131	8.7060
	1	0	0.5065	0.3317	0.1831	0.1774	0.2906	0.2242
		1	1.3555	0.6158	0.1262	0.1802	0.2378	0.4410
		2	4.3407	6.3206	6.2357	7.0961	2.2726	5.2529
	2	0	0.2998	0.1941	0.1208	0.0547	0.1275	0.3779
		1	1.1617	0.6579	0.2795	0.2398	0.5222	0.8681
		2	4.2160	5.2480	0.3368	0.3719	0.3337	0.9302
	3	0	0.1934	0.1083	0.0724	0.0523	0.0308	0.0622
		1	0.8688	0.4819	0.2690	0.1290	0.1237	0.4982
		2	1.9094	1.0190	0.3193	0.1109	0.3859	1.1002
	4	0	0.1383	0.0637	0.0399	0.0325	0.0305	0.0268
		1	0.6445	0.3140	0.1775	0.1270	0.0988	0.0602
		2	1.5445	0.8018	0.3405	0.1714	0.1029	0.3035
	5	0	0.1066	0.0405	0.0223	0.0174	0.0174	0.0198
		1	0.5052	0.2087	0.1079	0.0821	0.0814	0.0878
		2	1.2444	0.5794	0.2526	0.1760	0.1773	0.1619
	6	0	0.0865	0.0275	0.0131	0.0093	0.0088	0.0101
		1	0.4149	0.1452	0.0662	0.0479	0.0478	0.0568
		2	1.0310	0.4221	0.1689	0.1213	0.1314	0.1576
	7	0	0.0729	0.0198	0.0082	0.0052	0.0045	0.0049
		1	0.3523	0.1058	0.0423	0.0279	0.0262	0.0304
		2	0.8801	0.3159	0.1123	0.0764	0.0800	0.0979
	8	0	0.0630	0.0149	0.0054	0.0030	0.0024	0.0024
		1	0.3065	0.0801	0.0282	0.0168	0.0145	0.0158
		2	0.7690	0.2434	0.0764	0.0478	0.0468	0.0548
	9	0	0.0555	0.0116	0.0037	0.0018	0.0013	0.0012
		1	0.2714	0.0627	0.0195	0.0105	0.0083	0.0083
		2	0.6838	0.1925	0.0536	0.0305	0.0275	0.0302
	10	0	0.0497	0.0093	0.0027	0.0012	0.0007	0.0006
		1	0.2437	0.0504	0.0141	0.0068	0.0049	0.0045
		2	0.6162	0.1558	0.0388	0.0200	0.0166	0.0169

TABLE II. Numerical values of Δ_k for $c_0 = 3$ and $c_0 = 4.86$, multipole number L and overtone n . The values highlighted in red color correspond to the minimum value of Δ_k .

c_0	L	n	ω_1	ω_2	ω_3	ω_4	ω_5	ω_6	ω_7
0.96	0	0	-0.514	-1.123	-	-	-0.088	-1.031	-
		1	-0.995	-2.638	-	-	-2.219	-1.588	-
		2	-1.315	-4.270	-	-	-8.537	-2.579	-
	1	0	-0.459	-0.844	-	-	-0.663	-0.944	-1.970
		1	-1.011	-2.329	-	-	-	-	-
		2	-1.376	-3.841	-	-	-	-	-
	2	0	-0.416	-0.557	-	-	-0.936	-2.326	-
		1	-1.028	-1.964	-	-	-1.616	-3.821	-
		2	-1.456	-3.389	-	-	-	-	-
	3	0	-0.394	-0.452	-0.204	-0.167	-0.727	-1.698	-
		1	-1.043	-1.655	-	-	-1.919	-4.908	-
		2	-1.526	-3.028	-	-	-2.381	-6.706	-
	4	0	-0.382	-0.413	-0.277	-0.257	-0.530	-0.756	-
		1	-1.052	-1.442	-0.699	-0.383	-1.656	-3.816	-
		2	-1.583	-2.737	-	-	-2.622	-7.006	-
	5	0	-0.375	-0.394	-0.309	-0.299	-0.431	-0.482	-
		1	-1.059	-1.318	-0.842	-0.672	-1.396	-2.513	-
		2	-1.626	-2.507	-1.531	-0.306	-2.361	-5.555	-
	6	0	-0.371	-0.384	-0.327	-0.322	-0.389	-0.405	-0.100
		1	-1.063	-1.245	-0.919	-0.827	-1.233	-1.645	-
		2	-1.659	-2.333	-1.413	-0.857	-2.115	-4.085	-
	7	0	-0.368	-0.378	-0.337	-0.334	-0.371	-0.377	-0.248
		1	-1.067	-1.201	-0.964	-0.912	-1.146	-1.299	-0.135
		2	-1.684	-2.207	-1.491	-1.185	-1.950	-2.963	-
	8	0	-0.366	-0.373	-0.342	-0.341	-0.362	-0.365	-0.306
		1	-1.069	-1.173	-0.993	-0.962	-1.102	-1.168	-0.662
		2	-1.704	-2.117	-1.558	-1.376	-1.852	-2.319	-
	9	0	-0.365	-0.371	-0.346	-0.345	-0.359	-0.360	-0.330
		1	-1.071	-1.153	-1.012	-0.992	-1.081	-1.113	-0.863
		2	-1.718	-2.052	-1.607	-1.493	-1.799	-2.022	-0.824
	10	0	-0.364	-0.369	-0.349	-0.348	-0.357	-0.357	-0.342
		1	-1.072	-1.139	-1.026	-1.012	-1.071	-1.087	-0.955
		2	-1.731	-2.005	-1.643	-1.568	-1.771	-1.887	-1.280
1.5	0	0	-0.594	-1.163	-	-	-	-	-
		1	-1.179	-2.800	-	-	-	-	-
		2	-1.565	-4.539	-	-	-6.909	-2.289	-
	1	0	-0.536	-0.857	-	-	-0.491	-0.511	-1.543
		1	-1.201	-2.471	-	-	-	-	-0.719
		2	-1.644	-4.096	-	-	-	-	-
	2	0	-0.491	-0.608	-0.262	-0.199	-0.665	-1.086	-
		1	-1.226	-2.095	-	-	-1.331	-2.382	-2.123
		2	-1.744	-3.636	-	-	-	-	-
	3	0	-0.467	-0.519	-0.353	-0.325	-0.558	-0.699	-
		1	-1.246	-1.799	-1.132	-0.582	-1.558	-2.782	-
		2	-1.832	-3.271	-	-	-1.920	-4.213	-
	4	0	-0.455	-0.483	-0.389	-0.377	-0.482	-0.517	-0.105
		1	-1.260	-1.613	-1.144	-0.937	-1.461	-2.066	-
		2	-1.901	-2.988	-2.224	-0.815	-2.241	-4.099	-
	5	0	-0.448	-0.466	-0.406	-0.401	-0.450	-0.460	-0.313
		1	-1.269	-1.508	-1.192	-1.097	-1.371	-1.586	-0.448
		2	-1.954	-2.775	-2.012	-1.451	-2.226	-3.259	-
	6	0	-0.444	-0.456	-0.415	-0.412	-0.437	-0.441	-0.383
		1	-1.275	-1.446	-1.223	-1.175	-1.322	-1.402	-0.971
		2	-1.994	-2.622	-2.009	-1.739	-2.180	-2.648	-0.820
	7	0	-0.441	-0.450	-0.420	-0.418	-0.432	-0.434	-0.409
		1	-1.280	-1.408	-1.243	-1.216	-1.300	-1.333	-1.146
		2	-2.024	-2.515	-2.035	-1.888	-2.148	-2.357	-1.602
	8	0	-0.439	-0.446	-0.423	-0.422	-0.430	-0.431	-0.419
		1	-1.283	-1.382	-1.256	-1.240	-1.290	-1.306	-1.216
		2	-2.048	-2.439	-2.059	-1.972	-2.132	-2.229	-1.869
	9	0	-0.438	-0.443	-0.425	-0.425	-0.430	-0.430	-0.424
		1	-1.285	-1.365	-1.265	-1.255	-1.286	-1.294	-1.249
		2	-2.066	-2.384	-2.078	-2.023	-2.126	-2.175	-1.989
	10	0	-0.437	-0.441	-0.427	-0.426	-0.429	-0.430	-0.427
		1	-1.287	-1.352	-1.271	-1.265	-1.285	-1.289	-1.265
		2	-2.080	-2.344	-2.092	-2.057	-2.125	-2.151	-2.050

TABLE III. Numerical values of $Im(\omega_k)$ at each order k for $c_0 = 0.96$ and $c_0 = 1.5$. Entries with a dash indicate that the approach does not lead to a suitable value.

c_0	L	n	ω_1	ω_2	ω_3	ω_4	ω_5	ω_6	ω_7
3	0	0	-0.800	-1.394	-1.187	-0.793	-	-	-0.307
		1	-1.617	-3.439	-	-	-	-	-
		2	-2.156	-5.579	-	-	-6.751	-1.998	-
	1	0	-0.732	-1.088	-0.598	-0.334	-0.450	-0.351	-1.015
		1	-1.636	-3.120	-	-	-	-	-2.167
		2	-2.237	-5.160	-	-	-	-	-9.043
	2	0	-0.672	-0.821	-0.507	-0.440	-0.628	-0.662	-0.810
		1	-1.659	-2.718	-2.237	-1.342	-1.586	-1.416	-2.247
		2	-2.348	-4.670	-	-	-	-	-
	3	0	-0.637	-0.707	-0.538	-0.512	-0.628	-0.660	-0.513
		1	-1.679	-2.382	-1.792	-1.383	-1.762	-2.013	-1.824
		2	-2.452	-4.253	-3.694	-2.550	-2.683	-2.944	-3.046
	4	0	-0.617	-0.657	-0.556	-0.546	-0.605	-0.617	-0.520
		1	-1.693	-2.159	-1.709	-1.540	-1.789	-1.958	-1.561
		2	-2.538	-3.922	-3.168	-2.403	-2.810	-3.326	-2.880
	5	0	-0.606	-0.631	-0.566	-0.561	-0.591	-0.595	-0.550
		1	-1.703	-2.025	-1.705	-1.626	-1.770	-1.847	-1.606
		2	-2.606	-3.670	-2.953	-2.573	-2.883	-3.209	-2.672
	6	0	-0.598	-0.616	-0.571	-0.568	-0.584	-0.586	-0.566
		1	-1.710	-1.943	-1.712	-1.671	-1.753	-1.787	-1.666
		2	-2.658	-3.485	-2.890	-2.692	-2.894	-3.060	-2.712
	7	0	-0.594	-0.606	-0.573	-0.572	-0.581	-0.582	-0.572
		1	-1.716	-1.891	-1.718	-1.695	-1.743	-1.759	-1.699
		2	-2.699	-3.352	-2.873	-2.762	-2.890	-2.972	-2.779
	8	0	-0.590	-0.600	-0.575	-0.574	-0.579	-0.580	-0.575
		1	-1.719	-1.856	-1.722	-1.708	-1.738	-1.746	-1.715
		2	-2.731	-3.256	-2.871	-2.804	-2.886	-2.928	-2.823
	9	0	-0.588	-0.596	-0.576	-0.575	-0.579	-0.579	-0.577
		1	-1.722	-1.832	-1.725	-1.717	-1.736	-1.740	-1.723
		2	-2.756	-3.186	-2.872	-2.830	-2.884	-2.906	-2.848
	10	0	-0.586	-0.593	-0.576	-0.576	-0.578	-0.578	-0.577
		1	-1.724	-1.814	-1.727	-1.722	-1.734	-1.737	-1.728
		2	-2.772	-3.134	-2.874	-2.846	-2.883	-2.895	-2.862
4.86	0	0	-0.928	-1.546	-1.285	-1.049	-0.991	-0.542	-0.563
		1	-1.893	-3.855	-3.695	-3.653	-3.652	-3.392	-3.392
		2	-2.529	-6.253	-	-	-7.172	-2.505	-
	1	0	-0.856	-1.244	-0.793	-0.591	-0.569	-0.443	-0.859
		1	-1.907	-3.541	-3.270	-3.124	-3.117	-2.831	-2.860
		2	-2.607	-5.846	-	-	-6.747	-7.421	-8.604
	2	0	-0.786	-0.961	-0.644	-0.581	-0.683	-0.675	-0.913
		1	-1.927	-3.124	-2.630	-2.110	-2.114	-1.706	-2.345
		2	-2.719	-5.339	-	-	-	-	-
	3	0	-0.743	-0.827	-0.647	-0.622	-0.704	-0.714	-0.707
		1	-1.944	-2.761	-2.177	-1.837	-2.029	-2.073	-2.254
		2	-2.829	-4.889	-4.293	-3.676	-3.655	-3.464	-3.689
	4	0	-0.718	-0.766	-0.656	-0.645	-0.692	-0.700	-0.658
		1	-1.958	-2.508	-2.042	-1.884	-2.053	-2.136	-2.037
		2	-2.922	-4.524	-3.764	-3.207	-3.366	-3.533	-3.522
	5	0	-0.703	-0.733	-0.661	-0.656	-0.682	-0.685	-0.660
		1	-1.967	-2.351	-2.011	-1.934	-2.042	-2.091	-1.983
		2	-2.997	-4.240	-3.509	-3.187	-3.371	-3.539	-3.362
	6	0	-0.693	-0.714	-0.664	-0.661	-0.675	-0.677	-0.664
		1	-1.974	-2.253	-2.003	-1.962	-2.029	-2.052	-1.986
		2	-3.056	-4.029	-3.409	-3.231	-3.369	-3.471	-3.313
	7	0	-0.687	-0.702	-0.665	-0.664	-0.672	-0.673	-0.666
		1	-1.979	-2.190	-2.001	-1.978	-2.019	-2.030	-1.994
		2	-3.103	-3.876	-3.370	-3.266	-3.361	-3.416	-3.313
	8	0	-0.682	-0.694	-0.666	-0.665	-0.670	-0.670	-0.667
		1	-1.982	-2.147	-2.001	-1.987	-2.012	-2.018	-1.998
		2	-3.139	-3.764	-3.352	-3.289	-3.352	-3.382	-3.321
	9	0	-0.679	-0.689	-0.666	-0.666	-0.669	-0.669	-0.667
		1	-1.985	-2.117	-2.001	-1.992	-2.008	-2.011	-2.000
		2	-3.169	-3.682	-3.344	-3.304	-3.346	-3.363	-3.327
	10	0	-0.677	-0.684	-0.666	-0.666	-0.668	-0.668	-0.667
		1	-1.987	-2.095	-2.000	-1.995	-2.006	-2.007	-2.001
		2	-3.192	-3.620	-3.340	-3.313	-3.342	-3.351	-3.330

TABLE IV. Numerical values of $Im(\omega_k)$ at each order k for $c_0 = 3$ and $c_0 = 4.86$. Entries with a dash indicate that the approach does not lead to a suitable value.

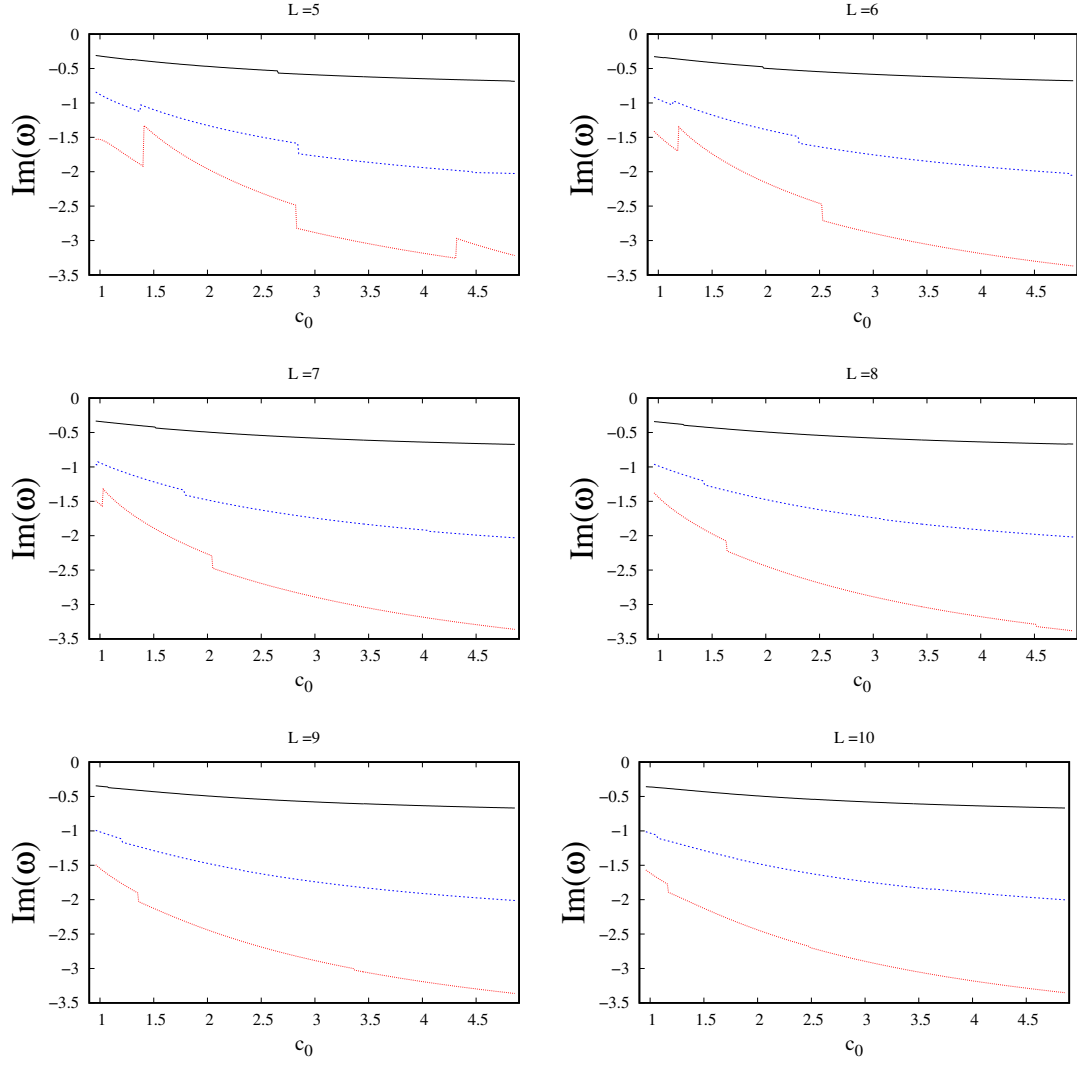


FIG. 2. Imaginary part of the QNM frequencies as a function of the free parameter c_0 for $L = 5, 6, \dots, 10$ and $n = 0$ (black line), $n = 1$ (blue line), $n = 2$ (red line).

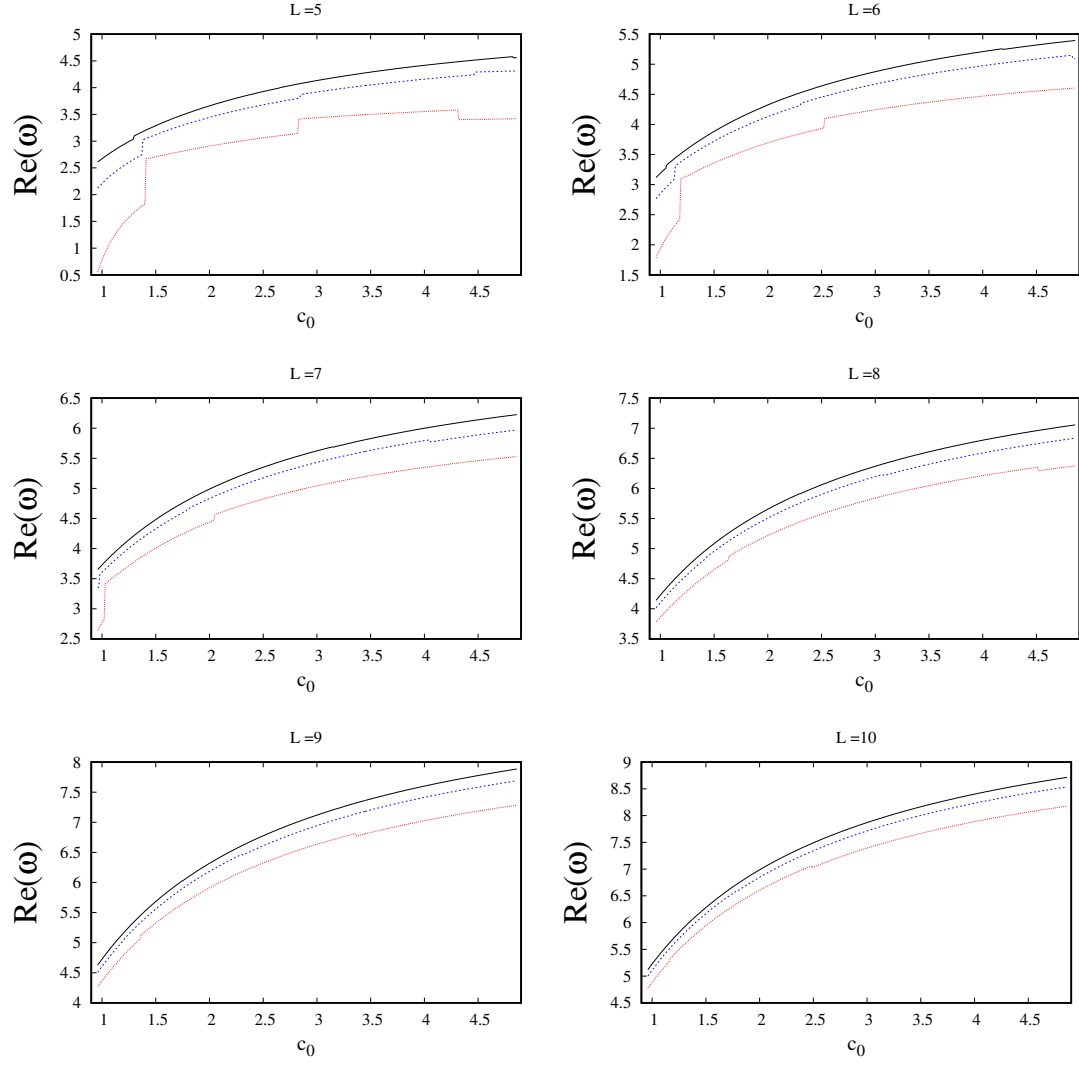


FIG. 3. Real part of the QNM frequency as a function of c_0 for $L = 5, 6, \dots, 10$ and $n = 0$ (black line), $n = 1$ (blue line), $n = 2$ (red line).